PHOTONIC SENSORS / Vol. 5, No. 1, 2015: 32–42

Study of Modeling Aspects of Long Period Fiber Grating Using Three-Layer Fiber Geometry

Amit SINGH*

Department of Electronics and Communication Engineering, Beant College of Engineering & Technology, Gurdaspur, Punjab, India

*Corresponding author: Amit SINGH E-mail address: er.amitsingh07@gmail.com

Abstract: The author studied and demonstrated the various modeling aspects of long period fiber grating (LPFG) such as the core effective index, cladding effective index, coupling coefficient, coupled mode theory, and transmission spectrum of the LPFG using three-layer fiber geometry. Actually, there are two different techniques used for theoretical modeling of the long period fiber grating. The first technique was used by Vengsarkar *et al* who described the phenomenon of long-period fiber gratings, and the second technique was reported by Erdogan who revealed the inaccuracies and shortcomings of the original method, thereby providing an accurate and updated alternative. The main difference between these two different approaches lies in their fiber geometry. Venserkar *et al* used two-layer fiber geometry which is simple but employs weakly guided approximation, whereas Erdogan used three-layer fiber geometry which is complex but also the most accurate technique for theoretical study of the LPFG. The author further discussed about the behavior of the transmission spectrum by altering different grating parameters such as the grating length, ultraviolet (UV) induced-index change, and grating period to achieve the desired flexibility. The author simulated the various results with the help of MATLAB.

Keywords: Long period fiber grating, three-layer fiber geometry, two-layer fiber geometry, transmission spectrum

Citation: Amit SINGH, "Study of Modeling Aspects of Long Period Fiber Grating Using Three-Layer Fiber Geometry," *Photonic Sensors*, 2015, 5(1): 32–42.

1. Introduction

Long period fiber gratings are fiber optic devices with numerous applications in optical communications and sensing systems. Fiber gratings are prepared by creating a region of periodically varying refractive index inside the core region of an optical fiber by using various techniques such as ultraviolet (UV) irradiation, ion implantation, irradiation by femtosecond pulses in the infrared, irradiation by CO_2 lasers, diffusion of dopants into the core, relaxation of mechanical stress and electrical discharges [1]. Fiber gratings are classified as the fiber Bragg grating (FBG) or long period fiber grating (LPFG) according to the grating period. An LPFG has a grating period in the range of 100 μm to 1 mm while an FBG has a sub-micron period. The LPFG was firstly presented by Vengsarkar *et al.* [2] as a band rejection optical filter in 1995. The LPFG promotes the coupling between the propagating core mode (i.e. the LP_{01} or HE_{11} mode presenting in the core of the single mode fiber) and co-propagating cladding modes (with m = 1, 2, 3, 4,⋯) in the perturbed region as shown in Fig. 1. The light coupled to the cladding modes decays quickly due to scattering losses, thus leaving lossy bands in the

Received: 23 March 2014 / Revised version: 26 September 2014
© The Author(s) 2014. This article is published with open access at Springerlink.com
DOI: 10.1007/s13320-014-0188-x
Article type: Regular

guided-core mode observed at the output end of the LPFG. Therefore, the transmission spectrum of the long period fiber grating has a series of attenuation bands at distinct peak resonant wavelengths, which satisfy the phase matching condition as [2].

$$\lambda_{\text{res}}^{m} = (n_{\text{eff},\text{co}} - n_{\text{eff,cl}}^{m})\Lambda \qquad (1)$$

where λ_{res} is the resonant wavelength, $n_{\text{eff,co}}$ is the effective refractive index of the core mode, $n_{\text{eff,cl}}^{m}$ is the effective refractive index of the mth cladding mode, and Λ is the grating period.

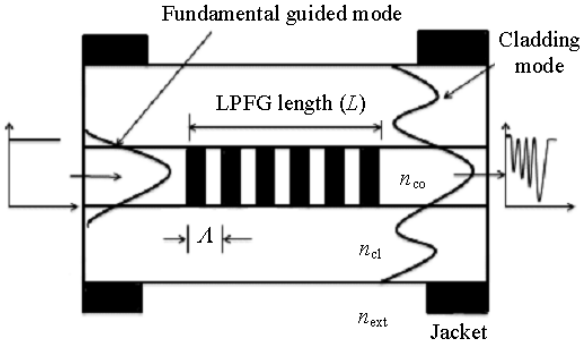

Fig. 1 Coupling of a fundamental guided mode to a cladding mode in the LPFG.

In optical communications, LPFG devices have been used for numerous applications such as in band-rejection filters [2], temperature and strain sensors [3], and any type of refractive index sensors [4, 5]. These sensors possess a number of benefits over other conventional sensors. For example, they are light and small in diameter, they have the good sensitivity and good long-term stability, and they are free from corrosion attack [6] and also from electromagnetic interference [7] that seriously affects many other conventional sensors. For employing the LPFG as any type of sensors (such as the refractive index sensor, temperature sensor, and strain sensor), they respond to shifts in various peak resonant wavelengths corresponding to various attenuation bands in the transmission spectrum of the LPFG, for example in the case of the temperature sensor, different temperatures of an external medium will give corresponding shifts in various peak resonant wavelengths corresponding to various attenuation bands of the transmission spectrum with respect to the original spectrum of the LPFG [8]. This is also the basis of using the LPFG as any type of sensors. Also the LPFG is much superior to the FBG as the refractive index sensor because the FBG is intrinsically insensitive to the external (surrounding) refractive index, since the light coupling takes place only between well-bound core modes that are well screened from the influence of the surrounding medium by the cladding layer. In order to use the FBG as a refractive index sensor, the cladding region is etched, so that an external medium acts as the cladding region. But by doing so, the FBG sensor loses its mechanical strength. Also in the LPFG sensors, there are several cladding modes which satisfy the phase matching condition so its transmission spectrum has a series of attenuation bands contrary to only one attenuation band in the case of the FBG sensor. In the LPFG sensors, by checking the wavelength shift of each attenuation band due to the variation in the parameter which is to be sensed, the required sensitivity can be obtained.

In the simplest term, the simulation procedure takes place as follows: firstly the propagation constants of the fundamental core and cladding modes are calculated to determine the effective refractive indices of the core and cladding modes, then the coupling coefficient is found for coupling between core mode and various cladding modes, and finally the complete transmission spectrum is obtained using the coupled mode theory.

2. General discussion regarding two-layer fiber geometry and three-layer fiber geometry

A review of the appropriate literature has shown that there are two different approaches existing for theoretical modeling of the LPFG. The first approach was proposed by Vengsarkar *et al*. [2] who described the new phenomenon of long period fiber gratings, and the second approach reported by Erdogan [9] revealed the inaccuracies and shortcomings of the

original method, thereby providing an updated and accurate method but resulting in the greater mathematical complexity. The key difference between these two approaches lies in their representations of the fiber geometry, which ultimately relied upon to derive discrete expressions for the dispersion relations, mode field profiles, and coupling coefficients. Whereas both methods employ the weakly guided approximation to find the effective refractive index of the fundamental core mode LP_{01}, and the two approaches differ in terms of the way in which the cladding effective refractive indices are calculated [9].

In weakly guided approximation, the normalized core-cladding index difference (Δ) is very low [9]:

$$\Delta = \frac{n_{co} - n_{cl}}{n_{co}} < 1. \quad (2)$$

The above assumption allows the simpler solution of the characteristic equations, which approximates the exact solutions [10]. The results in linearly polarized (LP) "pseudo modes" because the waves constructed from these simplified solutions propagate at small angles to the fiber axis and are essentially polarized in a single direction. Vengsarkar *et al.* employed this approach and ignored the effect of the core at the cladding ambient interface, so that a simple two-layer waveguide model would serve when describing the fiber cladding and ambient medium [2]. Whereas Erdogan [9] made use of the three-layer fiber geometry having exact vector field representations for the calculation of cladding modes. In this method, the effect of the core is not ignored when calculating the cladding effective refractive indices. In this paper, only those equations are discussed, which are helpful for theoretical modeling of the LPFG in the three-layer geometry to save the excessive mathematical complexity.

3. Calculation of core effective refractive index

The core effective refractive index is found from the LP mode dispersion relation in the form of an eigen value equation. In this approach, the inner cylinder is made up of core, and the outer cylinder is made up of the infinite and uniform cladding [2, 11], as shown in Fig. 2.

$$\frac{J_1(u_{co})}{J_0(u_{co})} = \frac{w_{co}}{u_{co}}\left(\frac{K_1(w_{co})}{K_0(w_{co})}\right) \quad (3)$$

where $J_0(u_{co})$ and $J_1(u_{co})$ are Bessel functions of the first kind of order zero and one, respectively, and $K_0(w_{co})$ and $K_1(w_{co})$ represent the modified Bessel functions of the second kind of order zero and one, respectively.

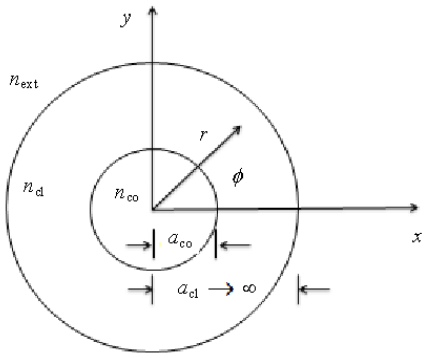

Fig. 2 Cross sectional view of an optical fiber, when calculating the core mode (the cladding diameter is assumed to be infinity).

u_{co} and w_{co} are normalized transverse wave numbers that can also be written in terms of the fiber's V number. The relation between u_{co} and w_{co} is as follows:

$$w_{co}^2 + u_{co}^2 = V^2. \quad (4)$$

Thus using the graphical approach, we can find the intersection point and corresponding value of u_{co} as shown in Fig. 3.

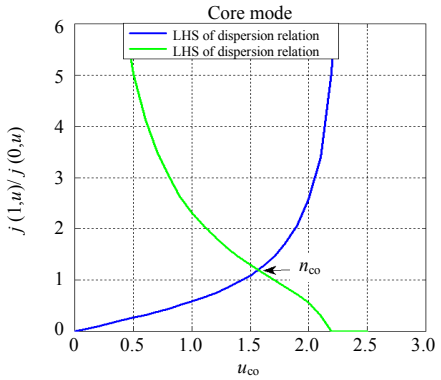

Fig. 3 Calculation of the core mode.

$$\beta_{co} = \sqrt{(fn_{co})^2 - \left(\frac{u_{co}}{a_{co}}\right)^2} \quad (5)$$

$$n_{eff} = \frac{\beta_{co}}{f}$$

where b is the normalized effective index and is used later:

$$b = \frac{n_{eff}^2 - n_{cl}^2}{n_{co}^2 - n_{cl}^2}$$

$$f = \frac{2\pi}{\lambda}$$

$$n_{cl} < n_{eff} < n_{co}$$

where f is the free space propagation constant.

Table 1 includes all the parameters used in various simulation procedures.

Table 1 Parameters used in simulation

Parameters	Values used
Core radius(a_{co})	4.65 μm
Cladding radius(a_{cl})	62.5 μm
Core refractive index(n_{co})	1.465
Cladding refractive index (n_{cl})	1.46
External refractive index (n_{ext})	1
Free space wavelength (λ)	1.310 μm

4. Calculation of cladding effective refractive indices using two-layer fiber geometry and three-layer fiber geometry

Calculation of various cladding modes using the two-layer fiber geometry is very similar to the procedure of determining the effective index of the core, so we will discuss this method first. Using the two-layer fiber geometry, we assume that the effect of the core is negligible at the cladding surrounding interface, so that a simple two-layer waveguide model will suffice when describing the fiber cladding and ambient medium. This approach is only possible when the presence of the core is ignored so that the fiber geometry once again comprises two concentric cylinders with a step-index profile as shown in Fig. 4. This time, the inner cylinder is a homogeneous solid consisting solely of the cladding material, whereas the outer cylinder is made up of the infinite but uniform medium surrounding the fiber.

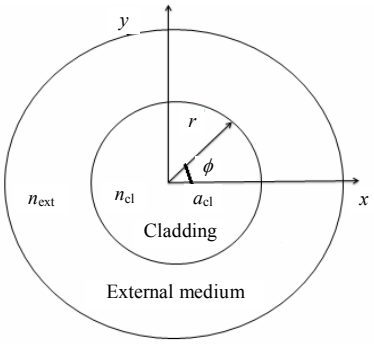

Fig. 4 Cross sectional view of an optical fiber, when calculating various cladding modes, in which the core region is ignored so that the cladding region acts as the core region and the external surrounding region acts as the cladding region.

Due to the large radius of the cladding a_{cl}, this model actually represents a simple multimode step-index fiber whose large-radius cladding region acts as the fiber core region, while the limitless external region acts as the cladding region [2, 11].

The rest of the technique of calculating cladding modes using the two-layer fiber geometry is very analogous to that of the calculation of the core mode.

The dispersion relation is used once again [see (3)], but due to the larger fiber dimensions, the graphical representation now yields numerous points of the intersection, each corresponding to one of several normalized transverse wave numbers belonging to a specific cladding mode, as shown in Fig. 5. Thus the propagation constant corresponding to each cladding mode order m can be determined from [11]. Using the two-layer fiber geometry, we

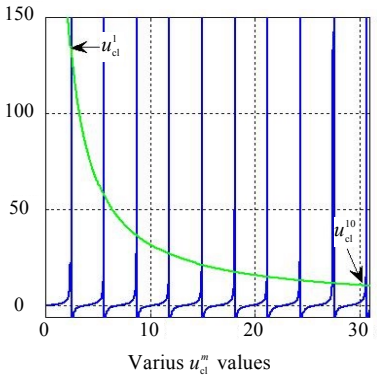

Fig. 5 Calculation of various effective refractive indices of the cladding using the two-layer fiber geometry (also called the graphical solution method).

employ the weakly guided approximation that Δ is very small, so the inaccuracy of this method is corrected by employing the three-layer fiber geometry. In this method, the core-cladding interface is not ignored, and the required dispersion relation for various cladding modes is given as [9]

$$\varsigma_0 = \varsigma_0' \tag{6}$$

where

$$\varsigma_0 = \frac{\dfrac{1}{\sigma_2}\left\{\left[JK + \left(\dfrac{\sigma_1\sigma_2 u_{21}u_{32}}{a_{co}a_{cl}n_{cl}^2}\right)\right]u_2 p_v(a_{cl}) - Kq_v(a_{cl}) + Jr_v(a_{cl}) - \dfrac{s_v(a_{cl})}{u_2}\right\}}{-\left[\left(\dfrac{u_{32}}{a_{cl}n_{cl}^2}\right)J - \left(\dfrac{u_{21}}{a_{co}n_{co}^2}\right)K\right]u_2 p_v(a_{cl}) + \dfrac{u_{32}q_v(a_{cl})}{a_{cl}n_{co}^2} + \dfrac{u_{21}r_v(a_{cl})}{a_{co}n_{co}^2}} \tag{7}$$

$$\varsigma_0' = \frac{\sigma_1\left\{\left[\left(\dfrac{u_{32}}{a_{cl}}\right)J - \left(\dfrac{u_{21}n_{ext}^2}{a_{co}n_{cl}^2}\right)K\right]u_2 p_v(a_{cl}) + \left(\dfrac{u_{32}q_v(a_{cl})}{a_{cl}}\right) + \left(\dfrac{u_{21}r_v(a_{cl})}{a_{co}}\right)\right\}}{\left[\left(\dfrac{n_{ext}^2}{n_{cl}^2}\right)JK + \left(\dfrac{\sigma_1\sigma_2 u_{21}u_{32}}{a_{co}a_{cl}n_{co}^2}\right)\right]u_2 p_v(a_{cl}) - \left[\dfrac{q_v(a_{cl})n_{ext}^2}{n_{co}^2}\right]K + Jr_v(a_{cl}) - \dfrac{s_v(a_{cl})n_{cl}^2}{u_2 n_{co}^2}} \tag{8}$$

$$\sigma_1 = j(vn_{eff}/Z_0) \tag{9}$$

$$\sigma_2 = j(vn_{eff}Z_0) \tag{10}$$

$$u_1 = \sqrt{\left(\frac{2\pi}{\lambda}\right)^2 (n_{co}^2 - n_{eff}^2)} \tag{11}$$

$$u_2 = \sqrt{\left(\frac{2\pi}{\lambda}\right)^2 (n_{cl}^2 - n_{eff}^2)} \tag{12}$$

$$w_3 = \sqrt{\left(\frac{2\pi}{\lambda}\right)^2 (n_{eff}^2 - n_{ext}^2)} \tag{13}$$

$$u_{21} = \frac{1}{u_2^2} - \frac{1}{u_1^2} \tag{14}$$

$$u_{32} = \frac{1}{w_3^2} + \frac{1}{u_2^2} \tag{15}$$

$$J = \frac{1}{2}\left(\frac{J_{v-1}(u_1a_{co}) - J_{v+1}(u_1a_{co})}{u_1 J_v(u_1a_{co})}\right) \tag{16}$$

$$K = -\frac{1}{2}\left(\frac{K_{v-1}(w_3a_{cl}) + K_{v+1}(w_3a_{cl})}{w_3 K_v(w_3a_{cl})}\right) \tag{17}$$

$$P_v(r) = J_v(u_2r)N_v(u_2a_{co}) - J_v(u_2a_{co})N_v(u_2r) \tag{18}$$

$$q_v(r) = \frac{1}{2}\{J_v(u_2r)[N_{v-1}(u_2a_{co}) - N_{v+1}(u_2a_{co})] - [J_{v-1}(u_2a_{co}) - J_{v+1}(u_2a_{co})]N_v(u_2r)\} \tag{19}$$

$$r_v(r) = \frac{1}{2}\{[J_{v-1}(u_2r) - J_{v+1}(u_2r)]N_v(u_2a_{co}) - J_v(u_2a_{co})[N_{v-1}(u_2r) - N_{v+1}(u_2r)]\} \tag{20}$$

$$S_v(r) = \frac{1}{4}\{[J_{v-1}(u_2r) - J_{v+1}(u_2r)][N_{v-1}(u_2a_{co}) - N_{v+1}(u_2a_{co})] - [J_{v-1}(u_2a_{co}) - J_{v+1}(u_2a_{co})][N_{v-1}(u_2r) - N_{v+1}(u_2r)]\}. \tag{21}$$

In all of above equations, $Z_0 = \sqrt{\mu_0/\varepsilon_0} = 377\Omega$ is the free space electromagnetic impedance. N is defined as a Bessel function of the second kind or the Neumann function, and the azimuthal order of the cladding mode is set to $v = 1$ in order for non-zero coupling to occur with the circularly symmetric core mode [9]. This approach directly provides cladding effective refractive indices by means of determining the intersection points in the graphical representation of the dispersion relation given in (6) and shown in Fig. 6.

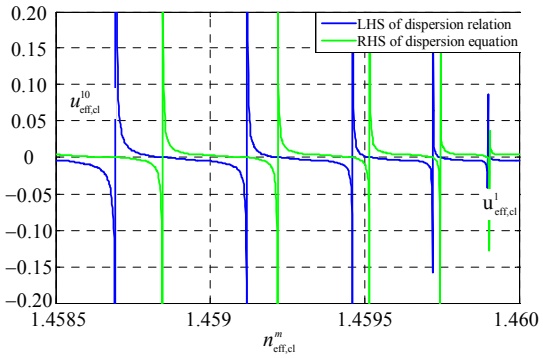

Fig. 6 Calculation of various effective refractive indices of the cladding employing the three-layer fiber geometry.

The cladding effective refractive indices of various cladding modes having different mode orders (m=1, 2, 3, 4,⋯) are obtained using both the two-layer fiber geometry and three-layer fiber geometry as shown in Table 2. From this table, we can estimate that as the cladding mode order

increases, there is an increase in deviation of results obtained by using the two-layer fiber geometry from the three-layer fiber geometry. Actually in order to use the LPFG as any type of highly sensitive sensors (such as the refractive index sensor, temperature sensor, and strain sensor), higher order cladding modes shows much higher sensitivity as compared to lower order cladding modes [1, 12]. So in order to achieve accurate results with the enhanced sensitivity for higher order cladding modes, the three-layer fiber geometry is best suited for studying the LPFG as any type of sensors.

Table 2 Effective refractive Indices of various cladding modes obtained by using the two-layer fiber geometry and three-layer fiber geometry for a typical set of fiber parameters given in Table 1.

Cladding mode order (m)	Using two-layer fiber geometry	Using three-layer fiber geometry
1	1.459903	1.459903
3	1.459716	1.459743
5	1.459155	1.459515
7	1.458295	1.458846
9	1.457134	1.4588468

5. Calculation of coupling coefficient between core mode and various co-propagating cladding modes in LPFG

Fiber gratings are inscribed to form a periodic refractive index profile in the core of an optical fiber. This causes a perturbation in the effective mode index of the principal guiding mode, given as follows [13]:

$$n_{\mathrm{co}}(z)=n_{\mathrm{co}}\left\{1+\sigma(z)\left[1+x\cos\left(\frac{2\pi}{\Lambda}z\right)\right]\right\} \quad (22)$$

where n_{co} is the unperturbed core refractive index, Λ is the period of the grating, x is the fringe visibility of the index change, where $0 \leqslant x \leqslant 1$, and $\sigma(z)$ is the slowly varying envelope of the grating.

If rearranging (22), we have

$$n_{\mathrm{co}}(z)=n_{\mathrm{co}}+n_{\mathrm{co}}\sigma(z)\left[1+x\cos\left(\frac{2\pi}{\Lambda}z\right)\right]. \quad (23)$$

This rearrangement tells us that the peak induced-index change at any z is given as $n_{\mathrm{co}}\sigma(z)[1+x]$ when $\cos\left(\frac{2\pi}{\Lambda}z\right)$ is equal to 1, and the minimum induced-index change at any z is given as $n_{\mathrm{co}}\sigma(z)[1-x]$ when $\cos\left(\frac{2\pi}{\Lambda}z\right)$ is equal to –1 with $n_{\mathrm{co}}\sigma(z)$ describing the profile of direct current (DC) induced-index change, averaged over the grating period.

In this perturbed region, the core mode couples its power presenting in LP_{01} mode to various co-propagating (co-propagating means propagating in the same direction) cladding modes (HE_{1m}). Erdogan [9] used exact field distributions in the LPFG modeling and thus coupling coefficient between the core mode LP_{01} (HE_{11}), and various cladding modes HE_{1m} are calculated using (24). In our analysis, the peak induced-index change is taken as $n_{\mathrm{co}}\sigma(z)=0.5\times10^{-4}$.

The only unknown quantity in (24) is the normalization constant E_{1m}^{cl}. We can calculate an expression for the normalization constant E_{1m}^{cl} once we determine the mode effective index by specifying that each mode carries a power of 1 W.

$$K_{1m-01}^{\text{cl-co}}(z)=\sigma(z)f\left(\frac{\pi b}{Z_0 n_{\mathrm{cl}}\sqrt{1+2b\Delta}}\right)^{\frac{1}{2}}\times \frac{n_{\mathrm{co}}^2 u_1}{u_1^2-\dfrac{v^2(1-b)}{a_{\mathrm{co}}^2}}\times\left(1+\frac{\sigma_2\varsigma_0}{n_{\mathrm{co}}^2}\right)\times E_{1m}^{\mathrm{cl}}\left[u_1J_1(u_1a_{\mathrm{co}})\times\frac{J_0V\sqrt{1-b}}{J_1(V\sqrt{1-b})}-\frac{V\sqrt{1-b}}{a_{\mathrm{co}}}J_0(u_1a_{\mathrm{co}})\right]. \quad (24)$$

When the integral is set equal to 1 W, as in (25), the only unknown in the resulting equation is the desired normalization constant [9].

$$P=\frac{1}{2}\mathrm{Re}\int_0^{2\pi}d\phi\int_0^{\infty}rdr(E_r^{\mathrm{cl}}H_\phi^{\mathrm{cl}*}-H_r^{\mathrm{cl}*}E_\phi^{\mathrm{cl}})=1W. \quad (25)$$

The integral along the radial direction can be divided into three portions. The first portion is the study of cladding modes vector components in the fiber core ($r \le a_{\mathrm{co}}$), and the cladding mode power in this region of operation is taken as P_1. The second portion is the study of cladding modes vector

components in the fiber cladding region ($a_{co} \le r \le a_{cl}$), and the cladding mode power in this region of operation is taken as P_2. The third portion is the study of cladding modes vector components in the surrounding region ($r \ge a_{cl}$), and the cladding mode power in this region of operation is taken as P_3.

The total power carried by the cladding modes is the sum of the powers carried in the core, the cladding, and the surrounding regions:

$$P = P_1 + P_2 + P_3 = 1 \text{ W} \tag{26}$$

where P_1, P_2, and P_3 can be calculated by means of the integral in (25) but with the limits along the radial direction replaced by those appropriate for the region of interest, and the results of these calculations are given as [9]

$$P_{1,\text{coeff}} = \frac{\pi a_{co}^2 u_1^2}{4}\left[\left\{\frac{n_{\text{eff}}}{Z_0} - \frac{n_{\text{eff}} z_0 \varsigma_0^2}{n_{co}^2} + \left(1 + \frac{n_{\text{eff}}^2}{n_{co}^2}\right)\right]\times [im(\varsigma_0)]\times [J_2^2(u_1 a_{co}) - J_1(u_1 a_{co}) J_3(u_1 a_{co})]\times \left[\frac{n_{\text{eff}}}{Z_0} - \frac{n_{\text{eff}} Z_0 \varsigma_0^2}{n_{co}^2} - \left(1 + \frac{n_{\text{eff}}^2}{n_{co}^2}\right)\times \text{Im}(\varsigma_0)\right]\times [J_0^2(u_1 a_{co}) + J_1^2(u_1 a_{co})]\right\} \tag{27}$$

$$P_1 = (E_{1m}^{\text{cl}})^2 P_{1,\text{coeff}} \tag{28}$$

$$P_{2,\text{coeff}} = \frac{\pi^3 a_{co}^2 u_1^4 u_2^2 J_1^2(u_1 a_{co})}{16}\times \left\{\left(\frac{n_{\text{eff}}}{Z_0} F_2^2 - \frac{n_{\text{eff}} Z_0}{n_{cl}^2} G_2^2\right)(Q + \bar{Q}) + \frac{1}{u_2^2}\times \left(\frac{n_{\text{eff}}}{Z_0} - \frac{n_{\text{eff}} Z_0 n_{cl}^2 \varsigma_0^2}{n_{co}^4}\right)(R + \bar{R}) + \left(1 + \frac{n_{\text{eff}}^2}{n_{cl}^2}\right) F_2 \text{Im}(G_2)(Q - \bar{Q}) + \left(1 + \frac{n_{\text{eff}}^2}{n_{cl}^2}\right)\frac{n_{cl}^2}{n_{co}^2 u_2^2}\text{Im}(\varsigma_0)(R - \bar{R}) - \left(1 + \frac{n_{\text{eff}}^2}{n_{cl}^2}\right)\left[\frac{n_{cl}^2 \text{Im}(\varsigma_0)}{n_{co}^2 u_2} F_2 + \frac{1}{u_2}\text{Im}(G_2)\right]\times (S - \bar{S}) + \frac{2 n_{\text{eff}}}{u_2}\times \left(\frac{Z_0 \varsigma_0}{n_{co}^2} G_2 - \frac{1}{Z_0} F_2\right)(S + \bar{S})\right\} \tag{29}$$

$$P_2 = (E_{1m}^{\text{cl}})^2 P_{2,\text{coeff}} \tag{30}$$

$$P_{3,\text{coeff}} = \frac{\pi^3 a_{co}^2 a_{cl}^2 u_1^4 u_2^4 J_1^2(u_1 a_{co})}{16 w_3^2 K_1^2(w_3 a_{cl})}\times \left\{\left[\frac{n_{\text{eff}} Z_0}{n_{\text{ext}}^2} G_3^2 - \frac{n_{\text{eff}}}{Z_0} F_3^2 - \left(1 + \frac{n_{\text{eff}}^2}{n_{\text{ext}}^2}\right) F_3 \text{Im}(G_3)\right]\times [K_2^2(w_3 a_{cl}) - K_1(w_3 a_{cl}) K_3(w_3 a_{cl})] + \left[\frac{n_{\text{eff}} Z_0}{n_{\text{ext}}^2} G_3^2 - \frac{n_{\text{eff}}}{Z_0} F_3^2 + \left(1 + \frac{n_{\text{eff}}^2}{n_{\text{ext}}^2}\right) F_3 \text{Im}(G_3)\right]\times [K_0^2(w_3 a_{cl}) - K_1^2(w_3 a_{cl})]\right\} \tag{31}$$

$$P_3 = (E_{1m}^{\text{cl}})^2 P_{3,\text{coeff}} . \tag{32}$$

Adding (28), (30), and (32), we get

$$P_1 + P_2 + P_3 = (E_{1m}^{\text{cl}})^2 [P_{1,\text{coeff}} + P_{2,\text{coeff}} + P_{3,\text{coeff}}]. \tag{33}$$

The total power is equal to 1 W as given in (26). So by using this result in (33), we get

$$E_{1m}^{\text{cl}} = \sqrt{\frac{1}{P_{1,\text{coeff}} + P_{2,\text{coeff}} + P_{3,\text{coeff}}}}. \tag{34}$$

The various unknown quantities used in power calculation coefficients ($P_{1,\text{coeff}}, P_{2,\text{coeff}}$, and $P_{3,\text{coeff}}$) are expressed below:

$$Q = \theta_J N_1^2(u_2 a_{co}) + \theta_N J_1^2(u_2 a_{co}) - 2\theta_{\text{JN}} J_1(u_2 a_{co}) n_1(u_2 a_{co}) \tag{35}$$

$$\bar{Q} = \overline{\theta_J} N_1^2(u_2 a_{co}) + \overline{\theta_N} J_1^2(u_2 a_{co}) - 2\overline{\theta_{\text{JN}}} J_1(u_2 a_{co}) N_1(u_2 a_{co}) \tag{36}$$

$$R = \frac{1}{4}\theta_J [N_2(u_2 a_{co}) - N_0(u_2 a_{co})]^2 + \frac{1}{4}\theta_N [J_2(u_2 a_{co}) - J_0(u_2 a_{co})]^2 - \frac{1}{2}\theta_{\text{JN}} [N_2(u_2 a_{co}) - N_0(u_2 a_{co})]\times [J_2(u_2 a_{co}) - J_0(u_2 a_{co})] \tag{37}$$

$$\bar{R} = \frac{1}{4}\overline{\theta_J} [N_2(u_2 a_{co}) - N_0(u_2 a_{co})]^2 + \frac{1}{4}\overline{\theta_N} [J_2(u_2 a_{co}) - J_0(u_2 a_{co})]^2 - \frac{1}{2}\overline{\theta_{\text{JN}}} [N_2(u_2 a_{co}) - N_0(u_2 a_{co})]\times [J_2(u_2 a_{co}) - J_0(u_2 a_{co})] \tag{38}$$

$$S=\frac{1}{2}\theta_J N_1(u_2a_{co})[N_0(u_2a_{co})-N_2(u_2a_{co})]+\frac{1}{2}\theta_N J_1(u_2a_{co})[J_0(u_2a_{co})-J_2(u_2a_{co})]-\frac{1}{2}\theta_{JN}\{N_1(u_2a_{co})[J_0(u_2a_{co})-J_2(u_2a_{co})]+J_1(u_2a_{co})[N_0(u_2a_{co})-N_2(u_2a_{co})]\} \quad (39)$$

$$\overline{S}=\frac{1}{2}\overline{\theta_J} N_1(u_2a_{co})[N_0(u_2a_{co})-N_2(u_2a_{co})]+\frac{1}{2}\overline{\theta_N} J_1(u_2a_{co})[J_0(u_2a_{co})-J_2(u_2a_{co})]-\frac{1}{2}\overline{\theta_{JN}}\{N_1(u_2a_{co})[J_0(u_2a_{co})-J_2(u_2a_{co})]+J_1(u_2a_{co})[N_0(u_2a_{co})-N_2(u_2a_{co})]\} \quad (40)$$

$$\theta_J=a_{cl}^2[J_2^2(u_2a_{cl})-J_1(u_2a_{cl})J_3(u_2a_{cl})]-a_{co}^2[J_2^2(u_2a_{co})-J_1(u_2a_{co})J_3(u_2a_{co})] \quad (41)$$

$$\theta_N=a_{cl}^2[N_2^2(u_2a_{cl})-N_1(u_2a_{cl})N_3(u_2a_{cl})]-a_{co}^2[N_2^2(u_2a_{co})-N_1(u_2a_{co})N_3(u_2a_{co})] \quad (42)$$

$$\overline{\theta_J}=a_{cl}^2[J_2^2(u_2a_{cl})+J_1^2(u_2a_{cl})]-a_{co}^2[J_2^2(u_2a_{co})+J_1^2(u_2a_{co})] \quad (43)$$

$$\overline{\theta_N}=a_{cl}^2[N_2^2(u_2a_{cl})+N_1^2(u_2a_{cl})]-a_{co}^2[N_2^2(u_2a_{co})+N_1^2(u_2a_{co})] \quad (44)$$

$$\theta_{JN}=a_{cl}^2\{J_2(u_2a_{cl})N_2(u_2a_{cl})-\frac{1}{2}[J_1(u_2a_{cl})N_3(u_2a_{cl})]+[J_3(u_2a_{cl})N_1(u_2a_{cl})]\}-a_{co}^2\{J_2(u_2a_{co})N_2(u_2a_{co})-\frac{1}{2}[J_1(u_2a_{co})N_3(u_2a_{co})]+[J_3(u_2a_{co})N_1(u_2a_{co})]\} \quad (45)$$

$$\overline{\theta_{JN}}=a_{cl}^2[J_0(u_2a_{cl})N_0(u_2a_{cl})+J_1(u_2a_{cl})N_1(u_2a_{cl})]-a_{co}^2[J_0(u_2a_{co})N_0(u_2a_{co})+J_1(u_2a_{co})N_1(u_2a_{co})]. \quad (46)$$

Once the coupling coefficients have been determined to describe the transfer of the optical power from the core mode to each of the possible cladding mode configurations, the LPFG's transmission spectrum can be directly obtained.

6. Transmission spectrum

There are several different techniques employed for the calculation of the transmission spectrum such as the integral method, formula method, and transfer matrix method. The detailed comparison among the integral method, formula method, and transfer matrix method is given in [14]. In [14], the accuracy and complexity of each technique were computed. In our discussion, we have chosen the integral method as it gives the exact solution of the transmission spectrum but the computation is complex. Three main dips seen in this spectrum correspond to coupling to m=1, 3, 5 cladding modes. In this figure, we have not shown lower even cladding modes because coupling due to lower even cladding modes is very less as compared to lower odd cladding modes [9]. Now we will study the behavior of the transmission spectrum by altering different grating parameters such as the grating period, grating length, and induced-index change.

The most unique feature of the long period fiber grating is the flexibility they offered for achieving the desired spectral characteristics which can be achieved by altering various grating parameters such as the grating period, grating length, and induced-index change.

7. Study of the transmission spectrum behavior by altering the grating period

The transmission spectrum of the LPFG shown in Fig. 7 has a period of 455 μm. When we choose higher values of the grating period as shown in Figs. 8 and 9, we can see that the various resonant

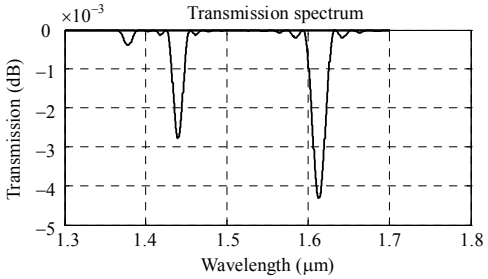

Fig. 7 Transmission spectrum of the long period fiber grating: the locations of various attenuation bands are located at 1.3780 μm, 1.4396 μm, and 1.6131 μm.

wavelengths correspond to various attenuation bands showing a red shift.

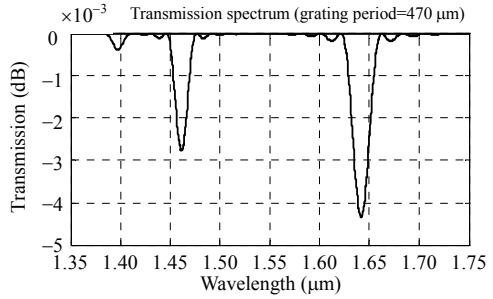

Fig. 8 Shifted transmission spectrum (grating period= 470 μm).

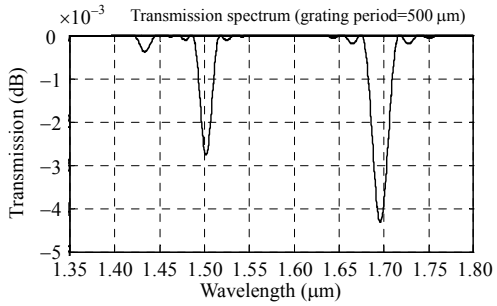

Fig. 9 Shifted transmission spectrum (grating period= 500 μm).

It is shown that the higher value of the grating period results in a corresponding increase in the resonant wavelength, and also the lower value of the grating period results in the lower value of the resonant wavelength, which is also reflected in Fig. 10. In other words, we can say that the grating period has a proportion relation with the resonant wavelength which is also realized from (1).

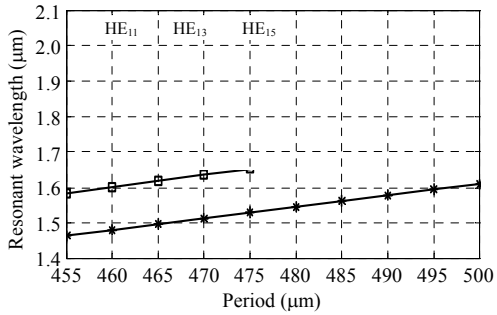

Fig. 10 Theoretical plots of resonant wavelength as a function of LPFG periodicity for lower odd cladding modes.

8. Study of the transmission spectrum behavior by altering the grating length

Now, we will discuss the behavior of the transmission spectrum by taking different values of grating lengths. The transmission spectrum shown in Fig. 7 has a grating length of 20 mm. When we choose the lower value of the grating length from 20 mm to 10 mm as shown in Fig. 11, the locations of various attenuation bands remain unchanged but the powers coupled to various cladding modes decrease, and also the bandwidths (thicknesses) of various attenuation bands increase [15]. A shorter grating length causes wide (thick) loss bands and creates small resonant peaks. On the other hand, when we choose the higher value of the grating length 60 mm as shown in Fig. 12, the coupling to various cladding modes increases, and also the bandwidths of various attenuation bands decrease. A longer grating length causes narrower loss bands and creates deeper resonant peaks. Figure 13 illustrates the relationship between the coupling depth and grating length. In this figure, it is verified that when we increase the grating length, the coupling depth becomes deeper.

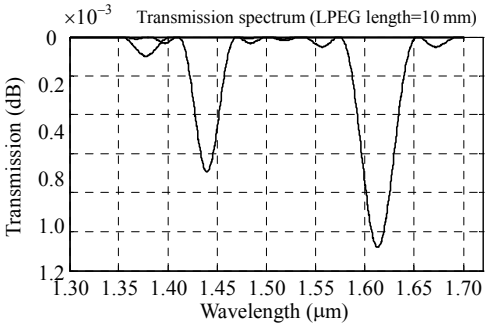

Fig. 11 Transmission spectrum (grating length=10 mm).

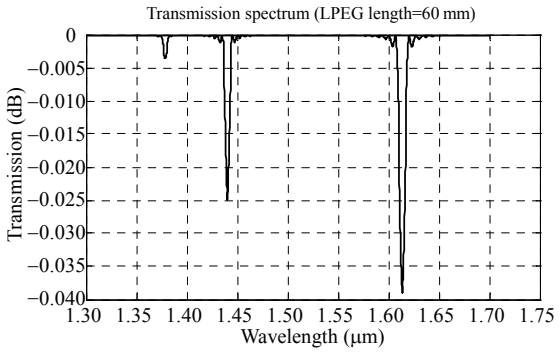

Fig. 12 Transmission spectrum (grating length=60 mm).

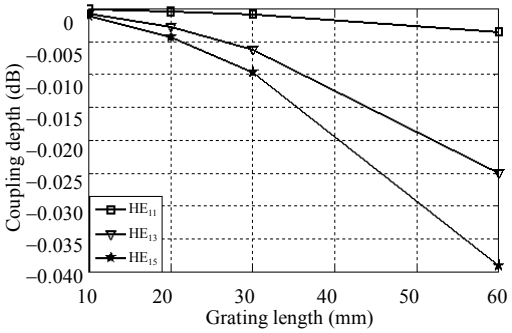

Fig. 13 Coupling depth as a function of the grating length for lower odd cladding modes.

9. Study of the transmission spectrum behavior by altering UV induced-index change

The LPFG is usually formed in the photosensitive single-mode fiber by the illumination of the core material with UV light. A long period fiber grating, which has restricted exposure of UV irradiation, has limited induced-index change, which results in a low coupling coefficient, which further results in low resonant peaks as shown in Figs. 7 and 14. Whereas, a long period fiber grating, which has prolonged exposure of UV-irradiation, has large induced-index change results in a large coupling coefficient, which further results in with deeper resonant peaks as shown in Fig. 15.

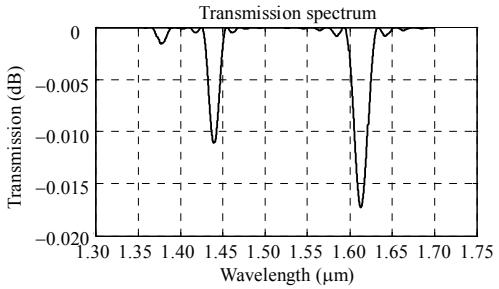

Fig. 14 Transmission spectrum (induced-index change = 0.5×10^{-4}).

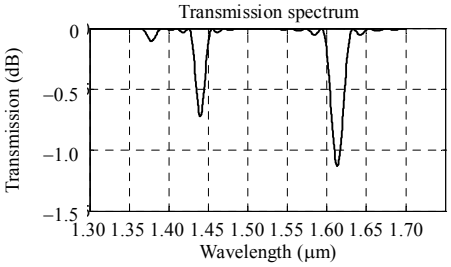

Fig. 15 Transmission spectrum (induced-index change = 4×10^{-4}).

Figure 16 shows the relationship between the coupling depth and induced-index change. From this graph, it is proved that the weaker grating has lower resonant peaks and the stronger grating has deeper resonant peaks.

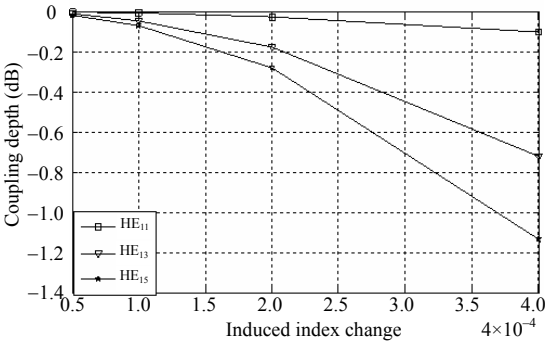

Fig. 16 Relationship between the coupling depth and induced-index change.

10. Conclusions

In this paper, the shortcomings of modeling employing the two-layer fiber geometry and theoretically modeled long period fiber grating using the three-layer fiber geometry are discussed. Using higher order cladding modes are an effective means of improving the sensitivity of the LPFG-based sensor. But there is a deviation of results obtained by using the two-layer fiber geometry from the three-layer fiber geometry as the cladding mode number increases due to weakly guided approximation in the two-layer fiber geometry, so the three-layer fiber geometry is the most updated and accurate method for theoretical modeling of the LPFG but results in the great mathematical complexity as compared to modeling using the two-layer fiber geometry. The influences of various physical parameters such as the grating period, grating length, and induced-index change on the transmission spectrum of the LPFG are also discussed. Choosing the appropriate grating period is helpful in attaining the desired resonant wavelength corresponding to desired attenuation bands. We can also modify the bandwidths and depths of various attenuation bands by choosing the appropriate grating length and UV induced-index

change. The effects of these parameters are very important because they are helpful in achieving the desired spectral characteristics for their efficient uses in any kind of sensor applications.

Open Access This article is distributed under the terms of the Creative Commons Attribution License which permits any use, distribution, and reproduction in any medium, provided the original author(s) and source are credited.

References

[1] S. W. James and R. P. Tatam, "Optical fiber long period grating sensors: characteristics and applications," *Measurement Science and Technology*, 2003, 14(5): 49–61.

[2] M. Vengsarkar, P. J. Lemaire, J. B. Judkins, V. Bhatia, T. Erdogan, and J. E. Sipe, "Long-period fiber gratings as band-rejection filters," *Journal of Lightwave Technology*, 1996, 14(1): 58–65.

[3] V. Bhatia, "Applications of long-period gratings to single and multi-parameter sensing," *Optics Express*, 1999, 4(11): 457–466.

[4] A. Singh, S. B. Rana, M. Singh, and A. Sharma, "Study and investigation of long period grating as refractive index sensor," *Optik – International Journal for Light and Electron Optics*, 2014, 125(7): 1860–1863.

[5] Q. Huang, Y. Yu, Z. Ou, X. Chen, J. Wang, P. Yan, *et al.*, "Refractive index and strain sensitivities of a long period fiber grating," *Photonic Sensors*, 2014, 4(1): 92–96.

[6] K. R. Cooper, J. Elster, M. Jones, and R. G. Kelly, "Optical fiber-based corrosion sensor systems for health monitoring of aging aircraft," in *IEEE Systems Readiness Technology Conference*, Valley Forge, pp. 847–856, 2001.

[7] J. A. Besley, T. Wang, and L. Reekie, "Fiber cladding mode sensitivity characterization for long-period gratings," *Journal of Lightwave Technology*, 2003, 21(3): 848–853.

[8] A. Singh, D. Engles, A. Sharma, and M. Singh, "Temperature sensitivity of long period fiber grating in SMF-28 fiber," *Optik – International Journal for Light and Electron Optics*, 2014, 125(1): 457–460.

[9] T. Erdogan, "Cladding-mode resonances in short- and long-period fiber grating filters," *Journal of the Optical Society of America A*, 1997, 14(8): 1760–1773.

[10] W. V. Etten and J. V. D Plaats, *Fundamentals of optical fiber communications*. New York: Prentice Hall, 1991.

[11] J. A. Buck, *Fundamentals of optical fiber*s. New York: John Wiley and Son Inc., 1995.

[12] K. W. Chung and S. Yin, "Analysis of a widely tunable long-period grating by use of an ultra thin cladding layer and higher-order cladding mode coupling," *Optics Letters*, 2004, 29(8): 812–814.

[13] T. Erdogan, "Fiber grating spectra," *Journal of Lightwave Technology*, 1997, 15(8): 1277–1294.

[14] Y. Yang and Z. Gu, "Comparing and analysis of calculation methods of long period fiber gratings transmission spectra," *Optik – International Journal for Light and Electron Optics*, 2013, 124(15): 2234–2240.

[15] A. van Brakel, "Sensing characteristics of an optical fibre long-period grating Michelson refractometer," DIng. Thesis, Rand Afrikaans University, 2004.